RSC Advances

Graphene prepared by gamma irradiation for corrosion protection of stainless steel 316 in chloride containing electrolytes

Journal:	*RSC Advances*
Manuscript ID:	RA-ART-06-2015-011287.R2
Article Type:	Paper
Date Submitted by the Author:	16-Aug-2015
Complete List of Authors:	Atta, Nada; Faculty of Science, University of Cairo, Egypt, Department of Chemistry Amin, Khaled; National Center for Radiation Research and Technology, Atomic Energy Authority, Physical Chemistry Abd El-Rehim, Hassan; National Center for Radiation Research and Technology, Atomic Energy Authority, Physical Chemistry Galal, Ahmed; Cairo University, Faculty of Science, Chemistry

Graphene prepared by gamma irradiation for corrosion protection of stainless steel 316 in chloride containing electrolytes

Nada F. Atta[1], Khaled M. Amin[2], Hassan A. Abd El-Rehim[2], Ahmed Galal[*1]

[1]Department of Chemistry, Faculty of Science, Cairo University, Al Gamaa Street, 12613 Giza, Egypt, tel.: +2002 35676561; fax: +2002 35727556, *e-mail: galal@sci.cu.edu.eg

[2]National Center for Radiation Research and Technology, Atomic Energy Authority, P.O. Box 29, Nasr City, Cairo, Egypt

Abstract

In this work we demonstrated the effective use of gamma irradiation for useful chemical conversion. Thus, graphene oxide was reduced to graphene upon exposure to gamma irradiation (GIG). The resulting graphene and steel-covered graphene were characterized using UV-Vis, XRD spectroscopies and FE-SEM. Corrosion protection of 316 stainless steel by GIG and gamma irradiated graphene/chitosan (GIG/CS) composite films in 3.5% NaCl solution was investigated using potentiodynamic polarization and electrochemical impedance spectroscopy. The protection efficiencies for GIG and GIG/CS were 82.2% and 89%, respectively. GIG/CS films over steel showed higher corrosion activation energy compared to GIG. EIS proved the stability of GIG and GIG/CS coatings after different immersion times in 3.5% NaCl solution. Coated surfaces were free from pits on the scale of magnification as demonstrated from SEM images. The pitting corrosion behavior of uncoated and GIG-coated surfaces was also studied.

Keywords

AISI 316; Graphene; Gamma irradiation; Corrosion protection; Natural polymers; Polarization; EIS.

1. INTRODUCTION

Stainless Steel is used in various sectors and wide range of applications because of its unique mechanical strength [1]. There are different grades of stainless steel among them, austenitic stainless steel (AISI 316). AISI 316 is widely used in nuclear power plants and different industries [2]. It has excellent properties such as corrosion and wear resistances, high tensile strength, and good impact [3, 4]. A protective film rich in chromium (oxides/hydroxides) covers the stainless steel surface which enhances its corrosion resistance [5]. But, Chromates are now heavily restricted in corrosion protection due to the high Toxicity of Cr (VI) and their carcinogenic effect [1, 6]. Moreover, chloride-containing solutions still represent an aggressive medium to this film layer and cause severe pitting corrosion [7].

The revolution of materials science allowed the development of smart and effective methods for corrosion protection [8, 9]. Graphene is considered one of the most important and extensively investigated materials for the last decade. Graphene, a two dimensional material, is a one atom thick structure consisting of hexagonal units of Sp^2- bonded carbon atoms [10- 15]. Nowadays, graphene has been introduced as an excellent anticorrosion material because of its unique characteristics such as excellent thermal and chemical stability, chemical inertness, high flexibility, impermeability to molecules even as small as helium, and remarkable mechanical properties [16- 20].

Several studies used graphene prepared by different techniques to develop coatings for corrosion protection of metals. For example Chen et al. [21] used graphene films formed by chemical vapor deposition (CVD) to prevent oxidation of (Cu and Cu/Ni alloys) substrates. Several publications reported the use of graphene prepared by CVD for corrosion protection of metals [22-27]. Guo et al. [28] reported the use of graphene/TiO_2 composite films prepared by a simple sol–gel method as coatings for AISI 304 and they exhibited increased photocathodic protection.

Recently, polymer/graphene composites have been widely used as anticorrosion coatings because of their superior passive properties resulting from coating matrix which act as a barrier and remarkable physical properties [17, 20, 29-32]. Chitosan (CS), which is a natural polymer, extracted from the polysaccharide chitin, is considered as a low cost, renewable marine polymer. Chitin is the second ubiquitous natural polysaccharide on earth and comes from the shells of crustaceans, such as shrimps and crabs. CS was introduced as candidate for ‘‘green’’ anticorrosion coatings because of its ability to form good barrier, specific solubility and versatile

chemical functionalization of chitosan [33, 34]. Some studies reported the use of CS for corrosion protection [35-36].

Most of the previous studies [21- 27] used expensive CVD for deposition of graphene on metals. Therefore, a novel route which combines the high purity of physical routes with convenience of chemical synthesis and economic benefits is economically and environmentally advantageous.

Gamma radiation (γ-radiation), electromagnetic radiation of high frequency, is one of the well-known ionizing radiation. Recently, reduction of graphene oxide using gamma irradiation (γ-irradiation) offers a promising "green" method for large scale and low-cost production of graphene. Furthermore, no chemicals or catalyst precursors are used which leads to a process with no chemical requirements or waste streams [37]. Few researchers reported the use of γ-radiation for reduction of graphene oxide [38- 39].

The aim of the present work is to use gamma irradiation as a safe and useful route to reduce graphene oxide to graphene and its application for protection of austenitic stainless steel 316 against corrosion in 3.5% sodium chloride electrolyte. The resulting graphene was also mixed with chitosan (GIG/CS) to form a composite that was also evaluated as an effective coating against corrosion for AISI 316. On one hand it was important to evaluate the extent of matrix holding of GIG to the natural polymer of CS, and on the other to evaluate its performance as coating protection against corrosion.

2. EXPERIMENTAL

2.1. Materials and Chemicals

All chemicals were used as received without further purification. Graphite powder with particle size distribution (<50 μm) was purchased from Merck (Frankfurter, Germany). Chitosan, sulfuric acid, acetic acid, sodium nitrate, potassium permanganate, hydrogen peroxide, hydrochloric acid and dimethylformamide (DMF) were supplied by Aldrich Chem. Co. (Milwaukee, WI. USA). AISI 316 (UNS 31600) stainless steel rods and sheets were provided by Goodfellow (USA). Stainless steel rods had diameters of 12 mm, and sheets were of thickness 0.1 mm.

2.2. Radiation Facility

The γ-ray irradiation was achieved using a ^{60}Co irradiation facility at dose rate 2.5 kGy/h. The irradiation facility was provided by The National Center for Radiation Research and Technology (NCRRT), Egyptian Atomic Energy Authority (EAEA).

2.3. Preparation of gamma irradiated graphene (GIG) and (GIG/CS) mixture

Graphene oxide (GO) was first prepared from graphite powder according to Hummers' method [40]. Thus, 1 g of graphite powder was added to 70 mL of concentrated H_2SO_4 at 0˚C. 0.5 g of sodium nitrate was slowly added to the mixture and vigorously stirred in an ice bath and 4.0 g of potassium permanganate was added to the suspension. The ice-bath was then removed and the temperature of the suspension is brought to 35^{o}C with stirring for 2 hours, then 50 mL of water was slowly added. The brown suspension was maintained at 98^{o}C for 15 minutes. The suspension was then further diluted with approximately 160 mL of water and treated with 30% hydrogen peroxide. The suspension turned into bright yellow color. Graphene oxide was then filtrated and washed several times with 5% HCl and water and left to dry.

Gamma irradiated graphene (GIG) was prepared by radiation induced reduction of GO. Thus, GO was dispersed in isopropanol/water (0.5 v/v %) mixture to obtain a final concentration of 1 mg/ mL GO dispersion. The as-prepared dispersion was sealed and exposed to ^{60}Co γ-ray source and realizing the condition of an absorbed dose 50 kGy with 2.5 kGy/h dose rate at room temperature. After the irradiation, the solution color was converted into black indicating the complete reduction of GO to graphene (G). The sample was washed with ethanol and distilled water and the irradiated graphene was left to dry. GIG suspension was obtained by dissolving 1.5 mg graphene in 1mL DMF.

To obtain GIG/CS hybrid, a 0.5% (mass ratio) chitosan solution was prepared by dissolving chitosan in 1.0% acetic acid solution then 10 μL of CS solution was added to the above GIG suspension.

2.4. Structural and surface characterization

UV-Vis absorption spectra were obtained by using Jasco V-550 UV-Vis spectrometer at room temperature. X-ray diffraction (XRD) analyses were performed on a Shimadzu machine (XRD-6000 series) with Cu-Kα radiation (λ = 1.54 Å), operated at 40 kV and 30 mA. XRD patterns were recorded in the range of 2θ = 4–90° (by steps of 0.02°). Scanning electron microscopy (SEM) measurements were performed on the surface of coated substrates to characterize the surface morphology using field-emission scanning electron microscope (FE-SEM) by a Quanta 250 FEG Field Emission Scanning Electron Microscope.

2.5. Substrate preparation and coating deposition

The substrate material used for the present investigation was 316 stainless steel alloy (AISI 316) which has the composition (wt %) indicated in table 1.

Insert Table 1

Specimens were in the form of sheets (1.0 mm thick) and rods. The sheets were used for the surface measurements while the rods were employed for electrochemical experiments. The test electrode which has cross-sectional area of 1.13 cm^2 was mechanically polished by emery papers to ensure the same surface roughness. This was followed by degreasing in acetone, rinsing with ethanol and drying in air. Aliquots of 10 μL of GIG suspension or GIG/CS mixture were added onto the surface of AISI 316 electrode. The electrode was left to dry at 60 ˚C (for 10 minutes) and finally exposed to the test solution.

2.6. Electrochemical cells and equipments

The cell used for electrochemical measurements was a typical three-electrode/one compartment glass cell. The working electrode was a 316 stainless steel alloy, reference electrode was Ag/AgCl (4.0 M KCl) and a Pt wire (5 cm long; diameter: 2 mm) as auxiliary electrode.

Electrochemical impedance spectroscopy measurements (EIS) were employed to monitor the corrosion performance of the coated 316 stainless steel substrates in a 3.5% NaCl solution. EIS measurements were carried out at the open circuit potential (OCP), using a Gamry-750 instrument and a lock-in-amplifier that are connected to a personal computer. The data analysis was provided with the instrument and applied non-linear least square fitting with Levenberg-Marquardt algorithm. All impedance experiments were recorded between 0.1 Hz and 100 kHz with an excitation signal of 10 mV amplitude.

The potentiodynamic polarization test was used to determine the overall corrosion behavior of the specimen. The potential of the electrode was swept at a rate of 1 mV/s from the initial potential (E_i) of -250 mV versus open circuit potential (OCP) to the final potential (E_f) of +250 mV versus OCP. Before the test, the electrode was left under open-circuit conditions until a steady corrosion potential value was reached.

Cyclic polarization experiments were used to determine the protection and pitting corrosion potentials. Experimental setup was as described for the potentiodynamic polarization text with an

initial potential (E_i) of +0.5 V, maximum potential (E_{max}) of +0.5 V and a final potential (E_f) of -0.5 V (vs. E_{OC}). All experiments were performed in controlled room temperature conditions at 25 °C ±0.2.

3. RESULTS AND DISCUSSION

3.1. Characterization of graphene

In order to ascertain that the conditions set during radiation of GO led to successful synthesis of the GIG, UV-Vis spectra and X-ray diffraction measurements have been used during different preparation stages. The UV–Vis spectra of graphene oxide and graphene are shown in Fig. 1. Both materials were dispersed in double distilled water until homogeneously distributed solutions were obtained. It is observed that the spectra shows a shoulder around 299 nm that corresponds to n→π* transition of C=O bonds for GO. This shoulder practically disappeared and the absorption peak around 239 nm corresponding to π →π* transitions of aromatic C–C bonds is red-shifted to 276 nm after irradiation which indicates the formation of graphene [41]. This is the first indication of the conversion of GO to GIG.

Insert Figure 1

X-ray diffraction patterns of the graphene oxide and graphene are shown in Fig. 2.The XRD pattern of GO shows a characteristic peak at 2θ value of 11.3 attributed to the expanded graphene oxide sheets and two weak graphite peaks at 23 and 42.3 due to the presence of some unreacted graphite [42]. After γ-irradiation, the intensity of the peak at 11.3 decreases significantly upon formation of GIG and a new dominant broad peak appears at 2θ value of about 26. The irregular stacking of some graphene layers makes the peak at 42.3 still appearing with low intensity in case of reduced GO. This indicates that the oxygen functional groups in the interlayer spacing of the graphene oxide had been removed during the reduction process [41, 43].

Insert Figure 2

Raman spectroscopy proved to be a standard reference testing protocol to ensure the formation of graphene. Supplement 1 depicts the Raman spectra of GO and GIG; The spectra show well referred documented D and G band peaks at 1346 cm^{-1} and 1585 cm^{-1} respectively [44]. After the irradiation, the I_D/I_G ratio increased substantially from 0.96 to 1.14 during the reduction of GO to graphene suggesting that the γ-ray irradiation alters the GO structure. Hence, the formation of

defects occurs beside the removal of oxide functional groups attached to the GO surface [45]. It can be explained that the irradiation induce the formation of many new graphitic domains in the structure, which are smaller in size, but more numerous in number.

The field-emission scanning electron microscope (FE-SEM) image in Fig. 3 shows the morphology of the as-prepared GIG. The GIG film showed a rippling structure with compact stacking over the AISI 316 substrate.

Insert Figure 3

3.2. Potentiodynamic polarization measurements

Fig. 4 shows the polarization curves of bare AISI 316, AISI 316 coated with GIG and AISI 316 coated with GIG/CS in 3.5% NaCl at room temperature (25 °C). The corrosion current densities were determined by extrapolating the linear part of the anodic and cathodic components of the curves. The results of the potentiodynamic polarization including corrosion potential (E_{corr}), corrosion current (i_{corr}), anodic and cathodic Tafel constants (β_a, β_c) and the protection efficiencies (PE) of GIG and GIG/CS are presented in Table 2.

Insert Table 2

The corrosion potential of GIG-coated stainless steel is -57.1 mV while that measured at bare AISI 316 is -183.1 mV. As indicated by the values of E_{corr}, a shift is observed to more positive potential in the anodic direction indicating more protection as the value mounts to more noble direction [46]. The i_{corr} value (0.0745 μA cm^{-2}) for the GIG-coated steel is remarkably lower than the corresponding value recorded for bare AISI 316 surface, ca. 0.4183 μA cm^{-2}. It is therefore concluded that the presence of GIG coating resulted in corrosion protection to the surface of steel. It is also important to relate the corrosion protection ability of graphene coating over AISI 316 to its large specific surface area, excellent mechanical properties and two-dimensional geometry of the graphene sheet. While graphene is expected to allow electronic conduction to the surface, but its hydrophobic nature and chemical inertness contributes to the isolation of the surface from electrolytic interactions. GIG/CS shows the lowest i_{corr} value (0.0462 μA/cm^2) indicating enhanced corrosion protection efficiency of the GIG/CS composite for the steel surface. It is therefore concluded that a synergistic effect with respect to corrosion protection of AISI 316 surface is expected when mixing CS to GIG to form the corresponding composite.

Moreover, the enhanced effect may be due to the well-dispersion of CS in the GIG matrix which hindered the diffusion pathways for oxygen and water molecules to the steel surface. The process

of steel corrosion involves several steps which depend on the presence of O_2 and H_2O for the dissolution of the steel and rust formation [29]. When the coating prevents O_2 gas molecules from reaching the surface, the coating becomes more effective for corrosion protection. Thus, when CS was inserted in the graphene matrix the diffusion pathway of O_2 and H_2O is hindered further resulting in more effective protection of steel surface against corrosion.

The protective efficiency (PE) of the coatings was determined using the following equation [47]:

$$PE = \left(1 - \frac{i_1}{i_\circ}\right) \times 100 \qquad (1)$$

Where i_o and i_1 are the corrosion current densities in absence and presence of the coating, respectively. It was observed that the PE increases from 82.2% in case of GIG coating to 89% when using GIG/CS composite.

Insert Figure 4

FE-SEM was used to examine the morphology of the stainless steel surface with and without coating as well as before and after exposure to the chloride solution under polarization conditions. The FE-SEM image in Fig. 5(a) shows the pitting on the surface of bare AISI 316 after immersion for 2 hours in 3.5 % NaCl solution and subjected to potentiodynamic polarization test. Fig. 5(b) and (c) show the surface morphology of AISI 316 coated with GIG and AISI 316 coated with GIG/CS, respectively after immersion for 2 hours in 3.5 % NaCl solution and subjected to potentiodynamic polarization test. After exposure and polarization of the electrode in sodium chloride, the GIG and GIG/CS coatings were removed to examine the surface of steel under the coatings. Fig. 5(d) and (e) show the morphology of the steel surface after removing the GIG and GIG/CS coatings, respectively. It is observed that the GIG and GIG/CS offer effective protection to the steel surface and no pitting spots were observed on the surface. It is important to mention that some “black” spots appeared in the images of the SEM that mainly corresponded to the most adherent parts of graphene after peeling the layer off the surface of steel.

Cyclic polarization measurements were conducted in order to determine the protection and pitting potentials for AISI 316, GIG-coated AISI 316 and GIG/CS-coated AISI 316 in 3.5% NaCl (the data are given in supplement 2). The pitting potential is determined from the value of potential at which the current increases. As shown in the supplement data, the reverse scan traces a hysteresis loop. The protection potential (or repassivation potential) was determined from the

value at which the loop closes on the reverse scan. The pitting potentials (E_{pit}) and protection potentials are difficult to estimate from the data of the supplement. However, the size of the loop of the hysteresis can be taken at this stage as an indication of the extent of pitting. Thus, the size of the loop decreases in the following order bare AISI 316 > GIG-coated steel > GIG/CS-coated steel in 3.5% NaCl. Sub-micro pitting is not excluded to take place on the coated surfaces.

Insert Table 3

3.3. Effect of temperature

The effect of temperature on the potential-current response of bare and coated steel surfaces was studied. Table 3 lists the parameters calculated from the effect of temperature measurements (E_{corr}, i_{corr}, β_a, β_c and PE) of bare steel, steel coated with GIG and GIG/CS, respectively.

Polarization parameters were estimated from experiments performed in 3.5%NaCl solution within temperature range of 298-328 K. The corrosion parameters indicated that as the temperature increases the values of i_{corr} increase and PE decrease. These data proved that the charge exchange of the corrosion process is under activation control. The data also showed that the effect of temperature on the i_{corr} values of the coated surface is less significant than that of bare surface. The results thus indicate the stability of GIG and GIG/CS coatings as the temperature of electrolyte increased.

The value of i_{corr} for bare steel increases 0.123 μA when the temperature increases from 298 to 328 K. On the other hand, the corresponding increase in current in case of GIG coating was 0.043 μA. The GIG/CS composite exhibited the least increase in i_{corr} value (0.039 μA). Visual inspection of the coating films showed that GIG and GIG/CS coatings retained their integrity and adhesion after exposure to NaCl solution at different temperatures.

The activation energy of the corrosion reaction is calculated from Arrhenius plots using the following equation [48]:

$$i_{corr} = Ae^{-Ea/RT} \qquad (2)$$

Where E_a is the activation energy, T is the absolute temperature, A is the frequency factor, R is the gas constant and (i_{corr}) is the corrosion current density.

Fig. 6 shows the relations between log i_{corr} versus 1/T for different surfaces. We calculated the values of E_a from the slopes of the straight lines relationships obtained in Fig. 6.

Insert Figure 5

The calculated values of the corrosion activation energy of bare AISI 316, GIG and GIG/CS were 2.92, 5.23 and 6.76 kJ mol^{-1}, respectively. These values agree with the order of protection efficiencies confirming the protective efficiency of GIG and GIG/CS. It is concluded that GIG/CS has improved the corrosion protection compared to GIG as the temperature increased.

Insert Figure 6

3.4. Electrochemical impedance spectroscopy (EIS)

In the potentiodynamic polarization, the electrochemical reaction occurring at the coating/electrolyte interface contributes to the polarization current so, it is advisable to study the corrosion protection performance of GIG or GIG/CS for extended exposures to sodium chloride solution. Thus, EIS measurement gives more information about the corrosion behavior of the different coatings under open-circuit conditions. The measurements were performed around the dynamic equilibrium potential using a small perturbation potential signal of 10 mV. A better understanding of the stability of the coatings and the surface/electrolyte interface is therefore anticipated.

The bare and graphene-coated stainless steel electrodes were immersed in NaCl solution (3.5 wt. %) for 0–120 minutes. EIS results are presented in the Nyquist format in order to monitor the protection ability of the coatings to the steel surface from corrosion. The magnitude of the impedance curves elevations recorded in the Nyquist format is a measure of the resistance of the surface against corrosion. Figure 7 shows Nyquist plots of bare stainless steel (a), stainless steel-coated with GIG (b) and stainless-steel coated with GIG/CS (c) after immersion for different times (10, 20, 30, 60 and 120 min) in the electrolyte solution (3.5% NaCl) at room temperature.

The two equivalent circuits in Fig. 8 were used to fit the EIS data. The equivalent circuit for the bare stainless steel surface (Fig. 8(a)) consists of the following elements: the solution resistance (R_s) between working and reference electrode, the passive film resistance (R_f) formed on the steel surface and the charge transfer resistance (R_{ct}). The capacitance was represented by the constant phase element (CPE) that is mainly connected with surface roughness of the corrosion product film and double-layer. The two circuit components CPE1 and CPE2 are constant phase elements representing two phase elements and n, and m are their corresponding exponents. Figure 8(b) shows the equivalent circuit for stainless steel coated with GIG and GIG/CS. In this

circuit R_s represents solution resistance. R_{coat} and C_{coat} represent the resistance and capacitance of the coating film, respectively. R_{ct} and C_{dl} represent the charge transfer resistance and double layer capacitance at the interface, respectively. Diffusion can create impedance known as the Warburg impedance (R_d) and could be attributed to mass transport during corrosion process. A schematic diagram of the simulated equivalent circuit with the surface structure is given in Supplement 3.

Important observations were noticed from the EIS data of Fig. 7. Thus, for bare stainless steel surface different elevations were observed in the impedance values with different times of immersion in the NaCl solution. On the other hand, suppressed semi-circles were observed at medium and high frequency regions that are followed by a diffusional component at lower frequencies for the coated electrodes. The capacitance nature of the GIG and GIG/CS coatings are well represented by the changes in the radius of suppressed semi-circles and the diffusion of the corrosion process is represented by the Warburg component.

Insert Figure 7

For the coated electrodes two frequency regions are observed, low frequency region and a high frequency region (cf. figures 7(b) and 7(c)). For the low frequency region a straight vertical line in the impedance plane is observed. This is represented by a series combination of resistance and capacitance (R-C) [49]:

$$Z(\omega) = \frac{R-j}{\frac{1}{2}\omega\, C} \qquad (3)$$

Where R represents resistance due to ionic conduction within the film layer, C is the internal capacitance and ω the angular velocity.

The high frequency region is characterized by a semicircle through the origin. This represented by a parallel combination of resistance and capacitance (R//C):

$$Z(\omega) = \frac{R}{1+\omega^2R^2C^2} - j\frac{\omega R^2 C}{1+\omega^2R^2C^2} \qquad (4)$$

The Warburg diffusive behavior that is usually observed in the low portion of the impedance spectra with a 45° inclination can be represented by a transmission line model according to the following equation:

$$Z_w = R_w \frac{coth\sqrt{i\omega\tau_d}}{\sqrt{i\omega\tau_d}} \qquad (5)$$

R_w is the effective distributed ionic impedance of the electrodes, τ_d is the diffusion time constant and ω is the angular frequency.

Assuming uniform distributed double layer capacitance behavior along the inner wall of the pore, a typical 45° Warburg type response in the complex plane would be expected. In the present case, in the low frequency portion of the impedance spectra in the complex plane of Figures 7(b) and 7(c) cannot be modelled using the classical finite space Warburg (FSW) impedance element given by equation (5). This could be explained in terms of the non-uniform diffusion properties of the electrodes depending on the pores size and shape.

The values of the fitting data of tables 4, 5 and 6 showed that the oxide film resistance (R_f) of bare surface is relatively higher than that formed over the coated surface (R_{coat}). The direct exposure of the surface to the electrolyte allowed oxide film growth compared to the graphene-coated surface. While the values of charge transfer resistance (R_{ct}) were higher for graphene-coated and graphene(CS)-coated stainless steel compared to the bare surface. For the uncoated electrode, R_f initially decreased after immersion and then followed a pattern of fluctuations thereafter. The coating resistance in case of GIG and GIG/CS (R_{coat}) showed less erratic variations namely in the case of CIG/CS that showed relatively higher values compared to GIG-coated electrodes. This is attributed to the effective protection imparted by the coating and the inclusion of CS within the graphene matrix, respectively. The charge transfer resistance is one order of magnitude higher in case of GIG and GIG/CS coated-stainless steel compared to the bare surface. This indicates better protection of the surface in case of stainless steel-coated electrodes. The variation in the charge transfer resistance, R_{ct}, for the bare electrodes showed systematic fluctuations of decrease and increase that reached a maximum value after two hours of immersion. It is expected that the "air-formed" oxide prior to immersion partially deteriorate due to chloride ions attack. Thus the value of charge transfer resistance decreased and is followed by an increase as the oxide build up was initiated. The values of R_{ct} showed relative stability with immersion time, namely in the case of the GIG/CS.

As depicted in Figures 7(b) and 7(c), the radius of the depressed semi-circle capacitive loop increased over the first 20 minutes (in case of GIG-coated electrode) and over the first 30 minutes (in case of GIG/CS-coated electrode). The radius increases again for the rest of exposure time to reach again a relatively lower value. The mass exchange through the graphene layer is more pronounced for coated steel samples. Again, the capacitive values of the film and for the

double layer charge showed relatively stable values throughout the immersion time for the coated surfaces. The graphene and graphene containing chitosan therefore imparts a protective layer for stainless steel against pitting corrosion in sodium chloride containing electrolytes. The FE-SEM micrographs showed no visual pit formation after graphene layer removal for samples immersed in chloride containing electrolytes.

Insert Figure 8

Insert Tables (4, 5 and 6)

4. Conclusions

Gamma irradiation induced reduction of graphene oxide intro reduced graphene (GIG). The produced material was used as a "green" and cheap route to obtain GIG and GIG/CS composite which offer protection for AISI 316 in 3.5% NaCl with enhanced efficiency. Polarization results showed that corrosion current densities (i_{corr}) values of stainless steel-coated GIG and GIG/CS composites are lower than that of bare stainless steel and these results were confirmed with EIS results. Polarization results showed that the effect of temperature on i_{corr} values of the coated steel is less significant than that of bare stainless steel indicating the stability of GIG and GIG/CS coatings at different temperatures. The activation energy values of GIG and GIG/CS are much higher than that of bare steel confirming that GIG and GIG/CS indicating enhanced corrosion protection as the temperature increases. EIS measurements showed that the coatings retain its corrosion resistance after different immersion times in NaCl solution. The FE-SEM images of the surface proved that the surface is pit-free for coated surfaces. Chitosan inclusion improved further the protection efficiency of the graphene layer.

Acknowledgement

The authors acknowledge the allowance of the use of the radiation facilities from the National Center for Radiation Research and Technology, Atomic Energy Authority of Egypt. We also thank the office of the Vice President for Research of Cairo University for partial financial support.

list of figures

list of tables

Table 6. Impedance parameters of GIG/CS after different immersion times in 3.5%NaCl at room temperature.

REFERENCES

[1] R. Zanda, K. Verbekenb, and A. Adriaens, *Prog. Org. Coat.*, 2011, **72**, 709–715.

[2] C. Carboni, P. Peyre, G. Beranger, and C. Lemaitre, *J. Mater. Sci.*, 2002, **37**, 3715-3723.

[3] O. Ogundare, B. Babatope, A. Adetunji, and S. Olusunle, *Miner. Mater. Charact. Eng.,* 2012, **11**, 914-918.

[4] M. A. Streicher, *Stainless Steels: Past, Present and Future*, Climax Molybdenum Co., Ann Arbor, Michigan, 1997.

[5] S. M. Hosseini, M. Salari, M. Ghasemi, and M. Abaszadeh, *Z. Phys. Chem.,* 2009, **223**, 769-779.

[6] W. Trabelsi, L. Dhouibia, E. Triki, M. G. Ferreira, and M. F. Montemor, *Surf. Coat. Technol.*, 2005, **192**, 284–290.

[7] A. Galal, N. F. Atta, and M. H. Al-Hassan, Mater. *Chem. Phys.,* 2005, **89**, 28–37.

[8] D. Shchukin and H. Möhwald, *Science*, 2013, **341**, 1458–1459.

[9] S. Lyon, *Nature*, 2004, **427**, 406–407.

[10] K. S. Novoselov, A. K. Geim, D. Jiang, V. Morozov, Y. Zhang, S. V. Dubonos, I. V. Grigorieva, and A. A. Firsov, *Science*, 2004, **306**, 666–669.

[11] P. Avouris and C. Dimitrakopoulos, *Mater. Tod.,* 2012, **15**, 86-97.

[12] Z. Xu, in *Physics and Applications of Graphene- Experiments*, ed. S. Mikhailov, InTechJaneza Trdine, Rijeka, Croatia, 2011, ch. 1, pp. 1-2.

[13] Z. Peralta-Inga, J. S. Murry, M. E. Grice, S. Boyd, C. J. O'Conner, and P. Politzer, *J. Mol. Struct. (Theochem),* 2001, **549**, 147-158.

[14] Y. Li, L. Tang, and J. Li, *electrochem. Commun*., 2009, **11**, 846–849.

[15] J. Wintterling and M. -L. Bocquet, *Surf. Sci*., 2009, **603**, 1841-1852.

[16] V. Berry, *Carbon*, 2013, **62**, 1–10.

[17] W. Sun, L. Wang, T. Wu, Y. Pan, and G. Liu, *Carbon*, 2014, **79**, 605–614.

[18] M. Topsakal, H. Sahin, and S. Ciraci, *Phys. Rev. B*, 2012, **85**, 155445.

[19] Hagar K. Hassan, Nada F. Atta, and Ahmed Galal, *Int. J. Electrochem. Sci*., 2012, **7**, 11161–11181.

[20] B. P. Singh, S. Nayak, K. K. Nanda, B. K. Jena, S. Bhattacharjee, and L. Besra, *Carbon*, 2013, **61**, 47–56.

[21] S. Chen, L. Brown, M. Levendorf, W. Cai, S. Ju, J. Edgeworth, X. Li, C. W. Magnuson , A. Velamakanni, R. D. Piner, J. Kang, J. Park, and R. S. Ruoff, *ACS Nano*, 2011, **5**, 1321–1327.

[22] A. Krishnamurthy,V. Gadhamshetty,R. Mukherjee, Z. Chen,W. Ren, H. Cheng, and N. Koratkar, *Carbon*, 2013, **56**, 45–49.

[23] Y. Zhao, Y. Xie, Y. Y. Hui, L. Tang, W. Jie, Y. Jiang, L. Xu, S. P. Lau, and Y. Chai, *J. Mater. Chem. C*, 2013, **1**, 4956–4961.

[24] G. Kalita, M. E. Ayhan, S. Sharma, S. M. Shinde, D. Ghimire, K. Wakita, M. Umeno, and M.Tanemura, *Corros. Sci*., 2014, **78**, 183–187.

[25] R. K. Raman, P. C. Banerjee, D. E. Lobo, H. Gullapalli, M. Sumandasa, A. Kumar, L. Choudhary, R. Tkacz, P. M. Ajayan, and M. Majumder, *Carbon,* 2012, **50**, 4040–4045.

[26] D. Prasai, J. C. Tuberquia, R. R. Harl, G. K. Jennings, and K. I. Bolotin, *ACS Nano*, 2012, **6**, 1102–1108.

[27] N. T. Kirkland, T. Schiller, N. Medhekar, and N. Birbilis, *Corros. Sci.,* 2012, **56**, 1–4.

[28] X. Guo, W. Liu, L. Cao, G. Su, H. Xu, and B. Liu, *Appl. Surf. Sci*., 2013, **283**, 498–504.

[29] C. Chang, T. Huang, C. Peng, T. Yeh, H. Lu, W. Hung, C. Weng, T. Yang, and J. Yeh, *Carbon*, 2012, **50**, 5044–5051.

[30] J. R. Potts, D. R. Dreyer, C. W. Bielawski, and R. S. Ruoff, *Polym. J.,* 2011, **52**, 5–25.

[31] Y. Yu, Y. Lin, C. Lin, C. Chan, and Y. Huang, *Polym. Chem.*, 2014, **5**, 535–550.

[32] K. Chang, M. Hsu, H. Lu, M. Lai, P. Liu, C. Hsu, W. Ji, T. Chuang, Y. Wei, J. Yeh, and W. Liu, *Carbon*, 2014, **66**, 144–153.

[33] S. Hirano, H. Inui, H. Kosaki, Y. Uno and T. Toda, in *Biotechnology and bioactive polymers*, ed. C.G. Gebelein and C.E Carraher, Plenum Press, New York, 1994, pp. 43-54.

[34] R. A. Ahmed, R. A. Farghali, and A. M. Fekry*, Int. J. Electrochem. Sci.*, 2012, **7**, 7270–7282.

[35] J. Carneiro, J. Tedim, S. C. Fernandes, C. S. Freire, A. Gandini, M. G. Ferreira, and M. L. Zheludkevicha*, ECS Electrochem. Lett.*, 2013, **2**, C19-C22.

[36] P. C. Rath, B. P. Singh, L. Besra, and S. Bhattacharjee, *J. Am. Ceram. Soc.*, 2012, **95**, 2725–2731.

[37] L. F. Dume´e, C. Feng, L. He, Z. Yi, F. She, Z. Peng, W. Gao, C. Banos, J. B. Davies, C. Huynh, S. Hawkins, M. C. Duke, S. Gray, P. D. Hodgson, and L. Kong, *Carbon*, 2014, **70**, 313–318.

[38] S. Wang, Y. Zhang, H. Ma, Q. Zhang, W. Xu, J. Peng, J. Li , Z. Yu, and M. Zhai, *Carbon*, 2013, **55**, 245–252.

[39] B. Zhang, L. Li, Z. Wang, S, Xie, Y. Zhang, Y. Shen, M. Yu, B. Deng, Q. Huang, C. Fan, and J. Li, *J. Mater. Chem.,* 2012, **22**, 7775–7781.

[40] W. S. Hummers and R. E. Offeman*, J. Am. Chem. Soc.,* 1958, **80**, 1339–1339.

[41] P. Sharma, G. Darabdhara, T. M. Reddy, A. Borah, P. Bezboruah, P. Gogoi, N. Hussain, P. Sengupta, and M. R. Das, *Catal. Commun.*, 2013, **40**, 139–144.

[42] A. Ansón-Casaosa, J.A. Puértolas, F.J. Pascual, J. Hernández-Ferrer, P. Castell, A.M. Benito, W.K. Maser, and M.T. Martínez, *Appl. Surf. Sci*., 2014, **301**, 264–272

[43] Z. Lei, L. Lu, and X. S. Zhao, *Energ. Environ. Sci.,* 2012, **5**, 6391–6399.

[44] A.C. Ferrari, J.C. Meyer, V. Scardaci, C. Casiraghi, M. Lazzeri, F. Mauri, S. Piscanec, D. Jiang, K. Novoselov, and A. K. Geim , *Phys. Rev. Lett*., 2006, **97**, 187401.

[45] S. Eigler, C. Dotzer, and A. Hirsch, *Carbon*, 2012, **50**, 3666–3673.

[46] D. A. Jones, in *Principles and prevention of corrosion*, ed. B. Stenquist, R. Kernan, and P. Daly, Prentice Hall, NJ, USA, 2nd ed., 1996, ch. 3, pp. 75-115.

[47] D. P. Le, Y. H. Yoo, J. G. Kim, S. M. Cho, and Y. K. Son, *Corros. Sci.,* 2009, **51**, 330–338.

[48] M.J. Bahrami, S.M.A. Hosseini, and P. Pilvar, *Corros. Sci.*, 2010, **52**, 2793–2803.

[49] M.E. Orazem, B. Tribollet, *Electrochemical impedance spectroscopy*, Wiley, NJ, USA, 2008, pp. 191-197.

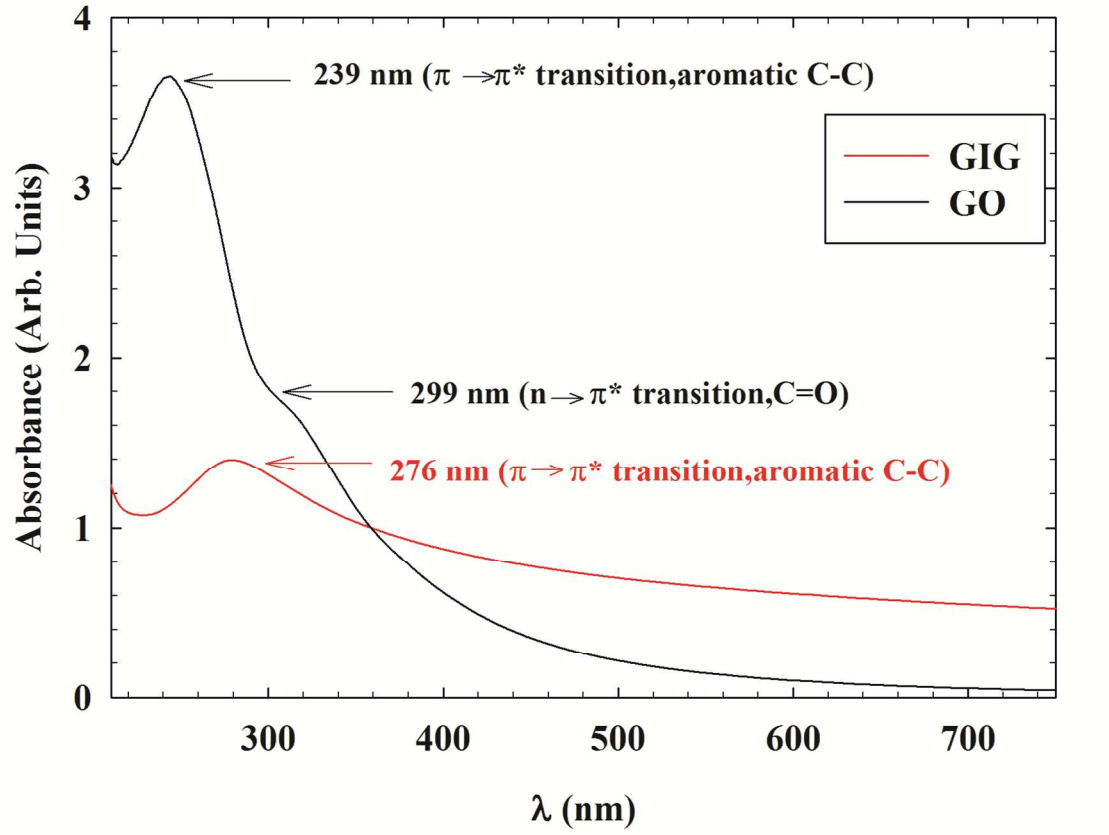
239 nm (π →π* transition,aromatic C-C)
299 nm (n→π* transition,C=O)
276 nm (π→π* transition,aromatic C-C)
GIG
GO
Absorbance (Arb. Units)
λ (nm)
0
1
2
3
4
300
400
500
600
700

Figure 1

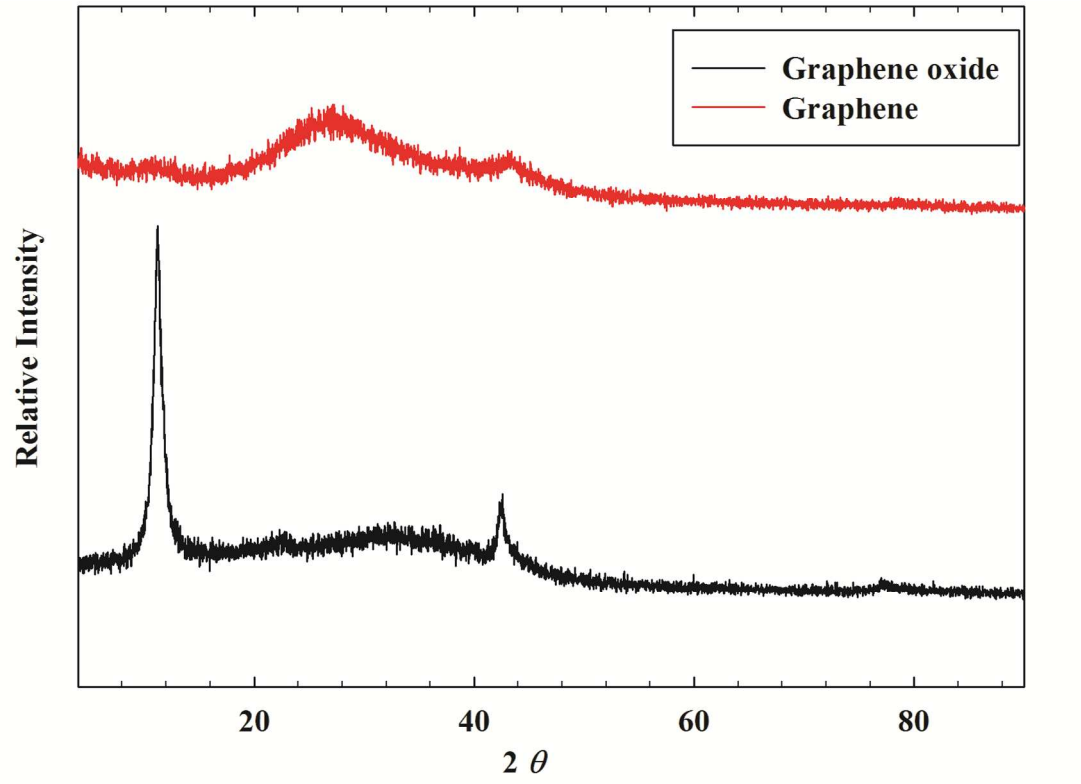

Figure 2

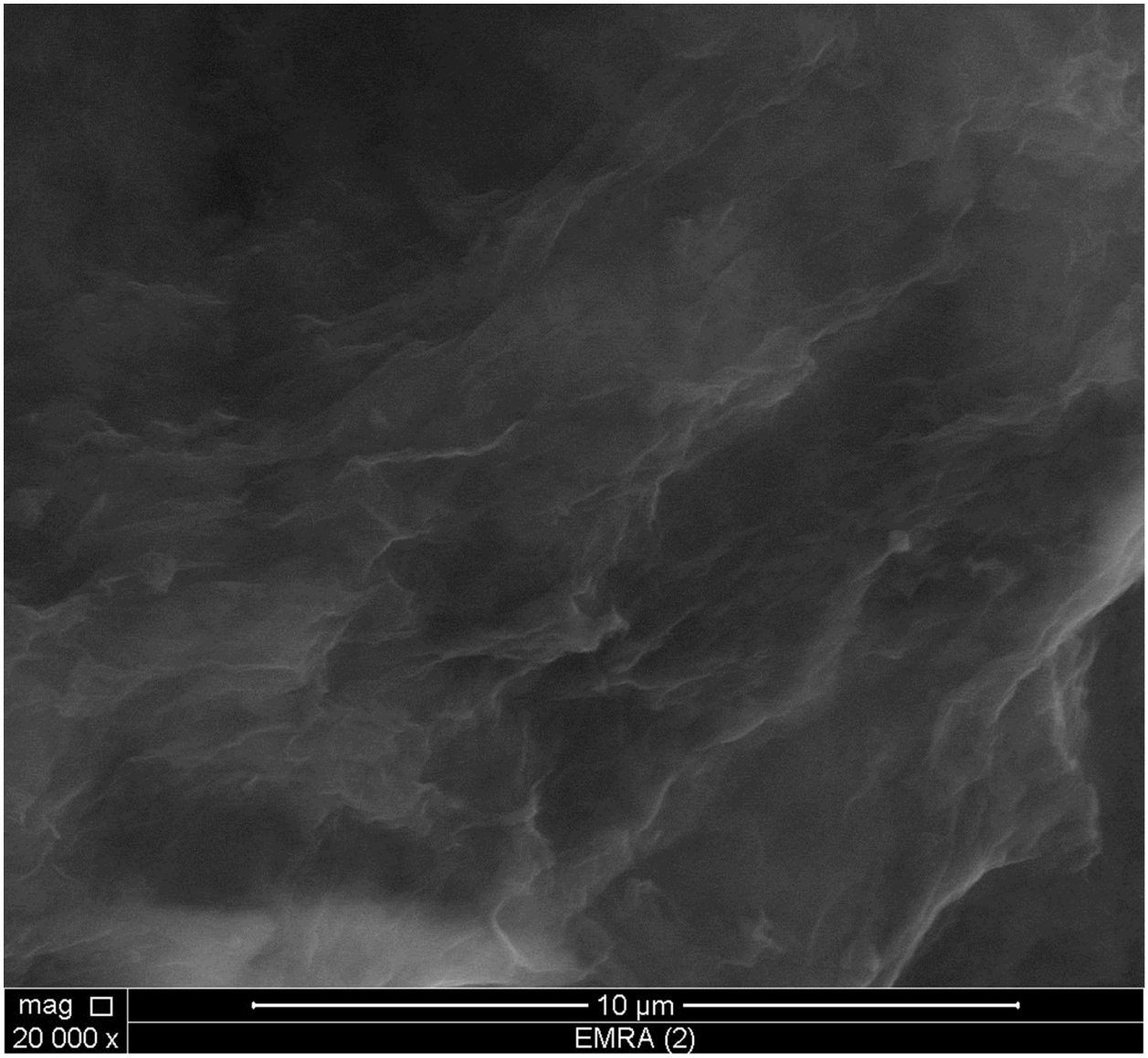

Figure 3

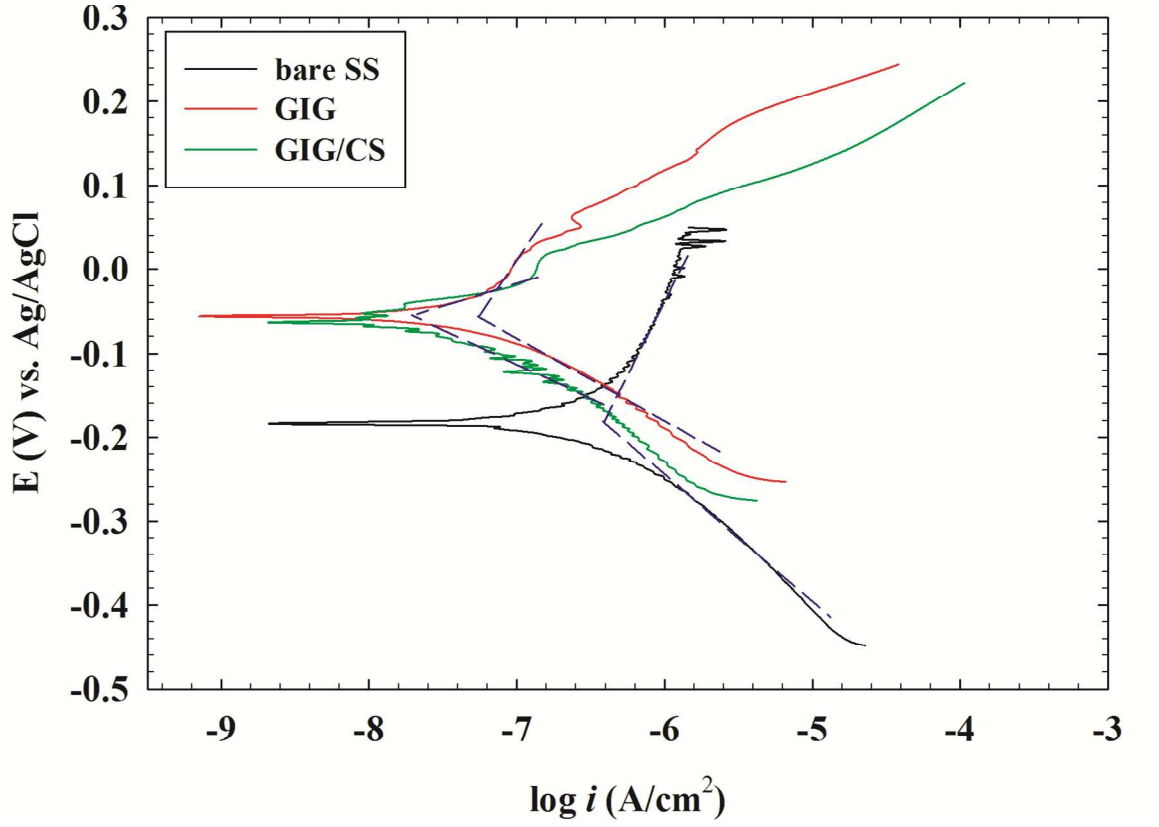
bare SS
GIG
GIG/CS
E (V) vs. Ag/AgCl
log i (A/cm2)
0.3
0.2
0.1
0.0
-0.1
-0.2
-0.3
-0.4
-0.5
-9
-8
-7
-6
-5
-4
-3

Figure 4

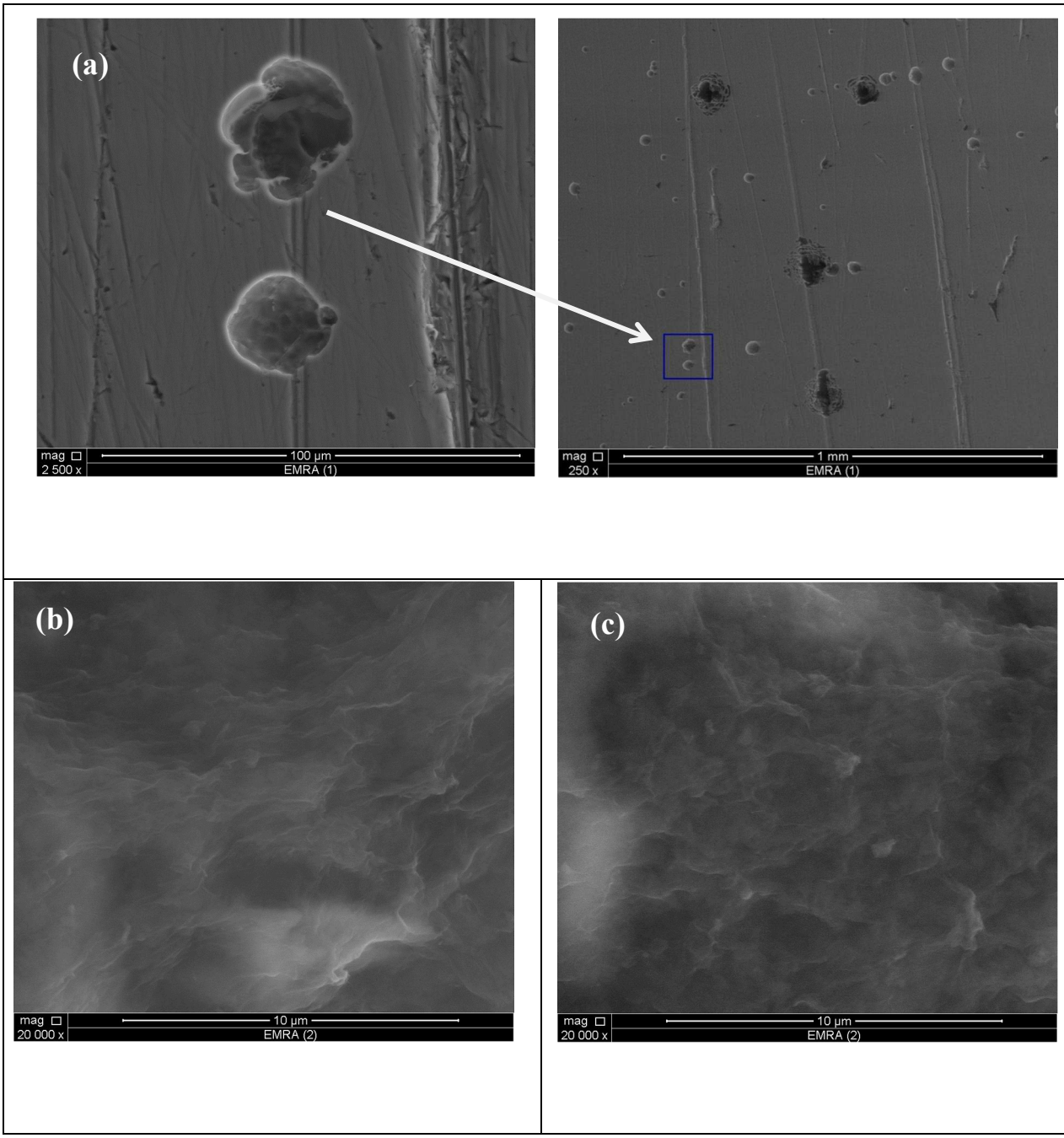
(a)
mag
2 500 x
100 µm
EMRA (1)
mag
250 x
1 mm
EMRA (1)
(b)
mag
20 000 x
10 µm
EMRA (2)
(c)
mag
20 000 x
10 µm
EMRA (2)

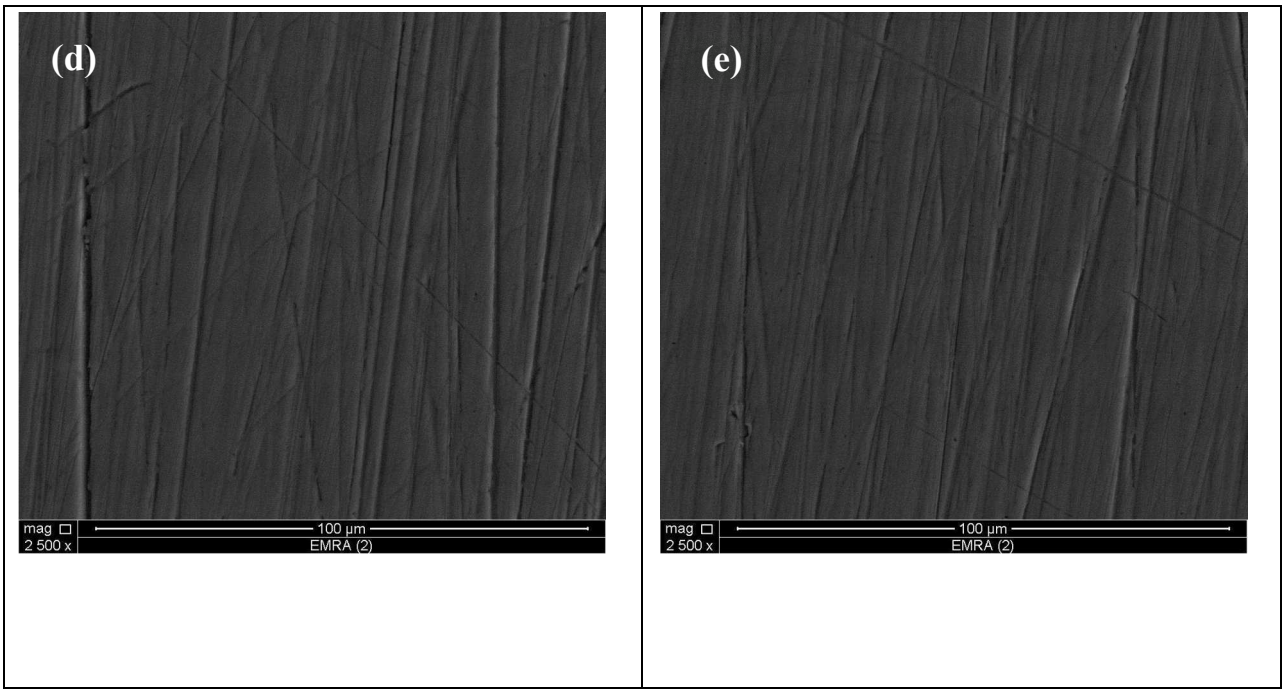

Figure 5

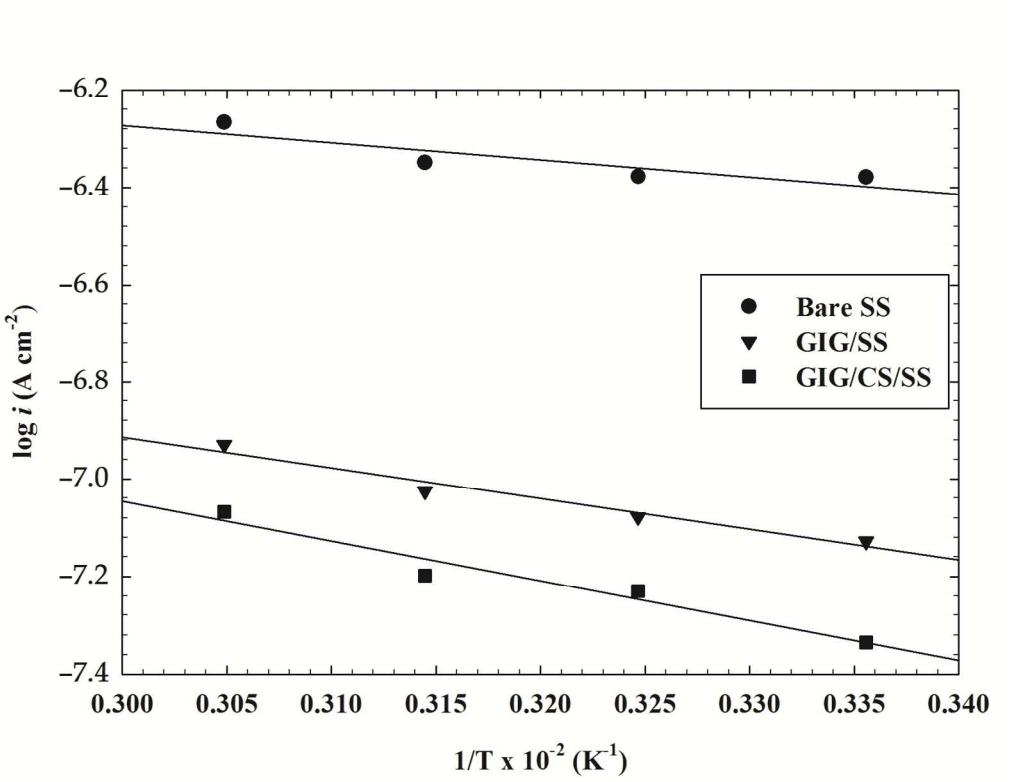

Figure 6

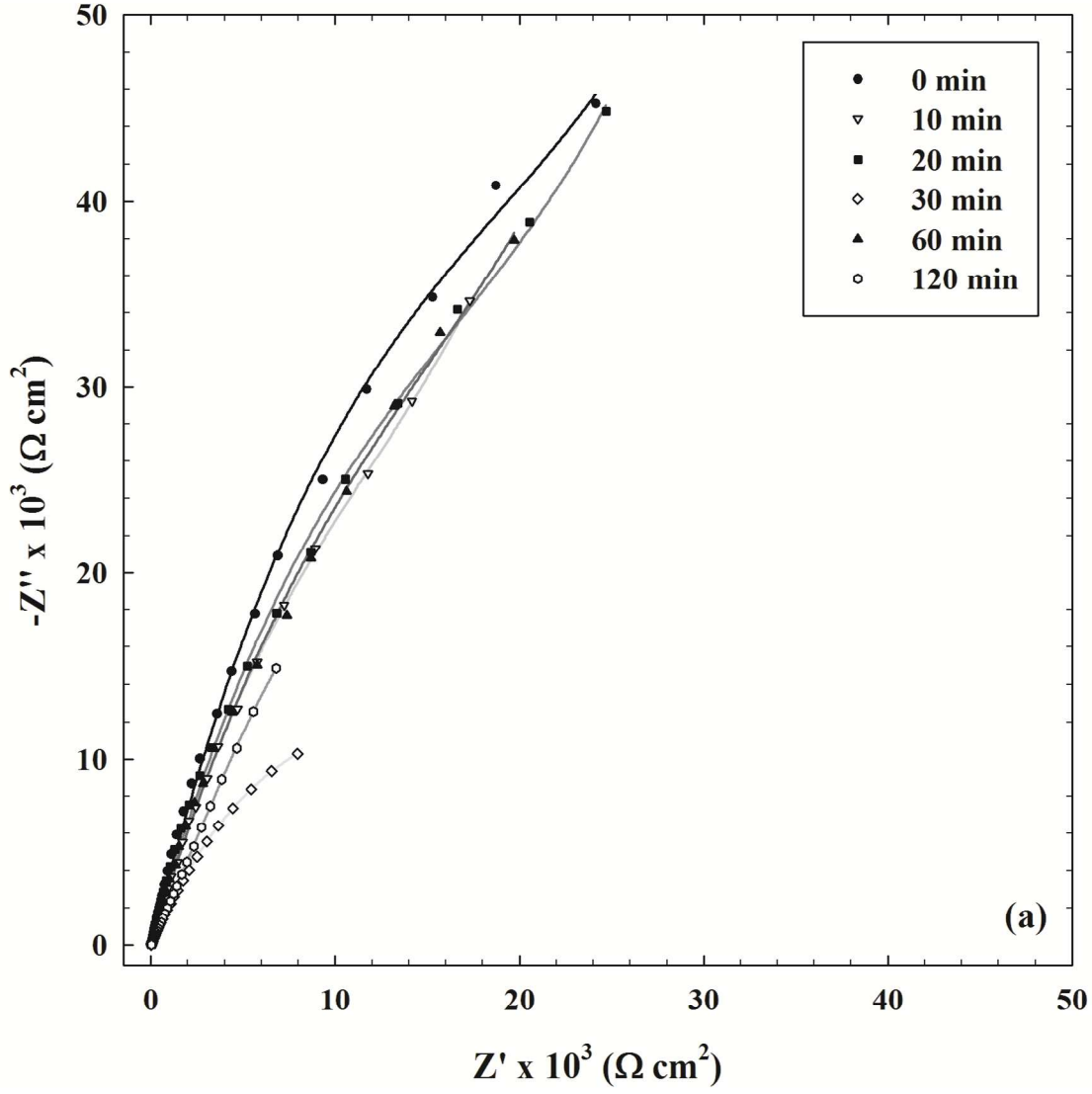
0 min
10 min
20 min
30 min
60 min
120 min
(a)
-Z'' x 10^3 (Ω cm^2)
Z' x 10^3 (Ω cm^2)
0
10
20
30
40
50

Figure 7a

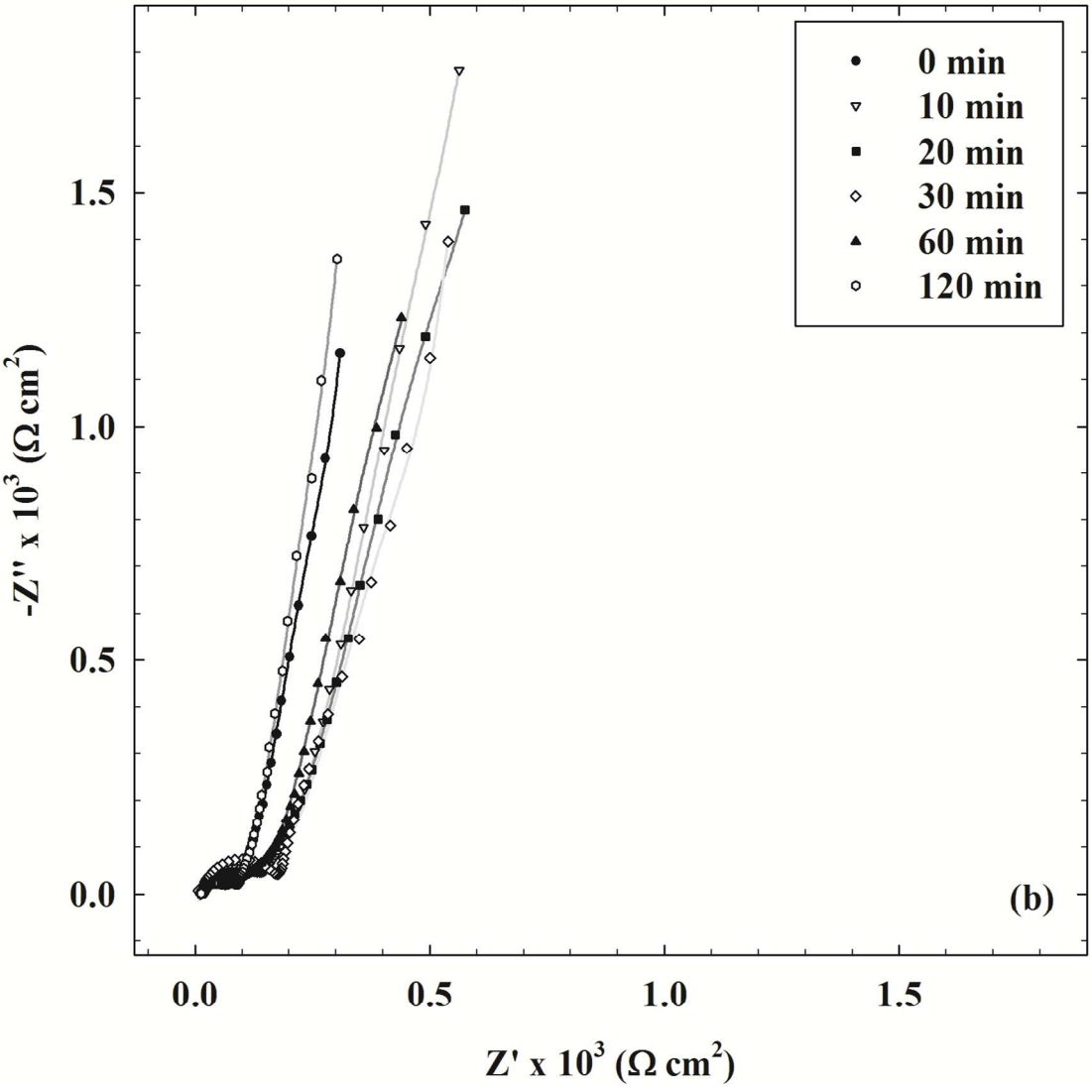
0 min
10 min
20 min
30 min
60 min
120 min
(b)
-Z'' x 10^3 (Ω cm^2)
Z' x 10^3 (Ω cm^2)
0.0
0.5
1.0
1.5

Figure 7b

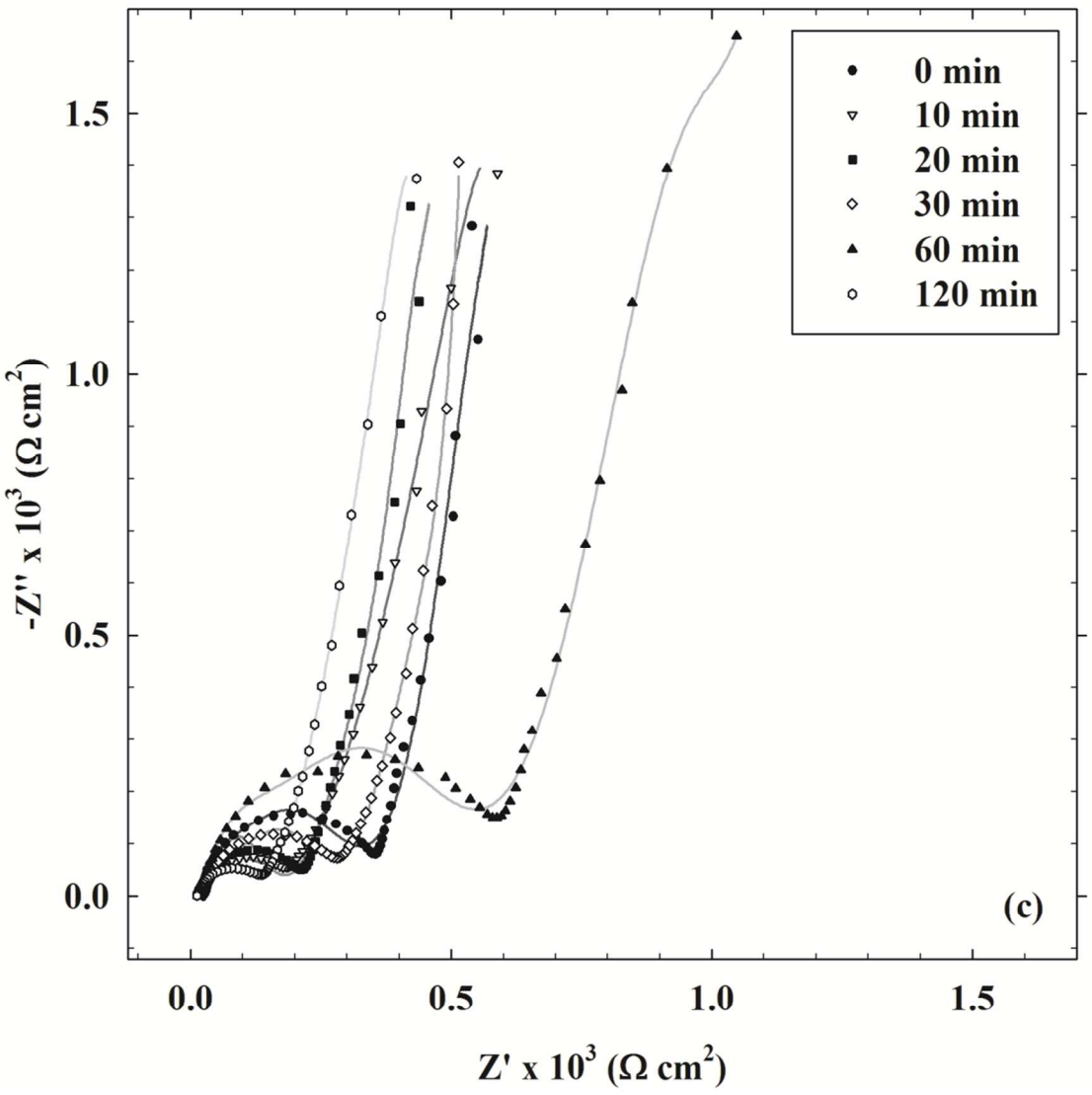
0 min
10 min
20 min
30 min
60 min
120 min
(c)
-Z'' x 10^3 (Ω cm^2)
Z' x 10^3 (Ω cm^2)
0.0
0.5
1.0
1.5

Figure 7c

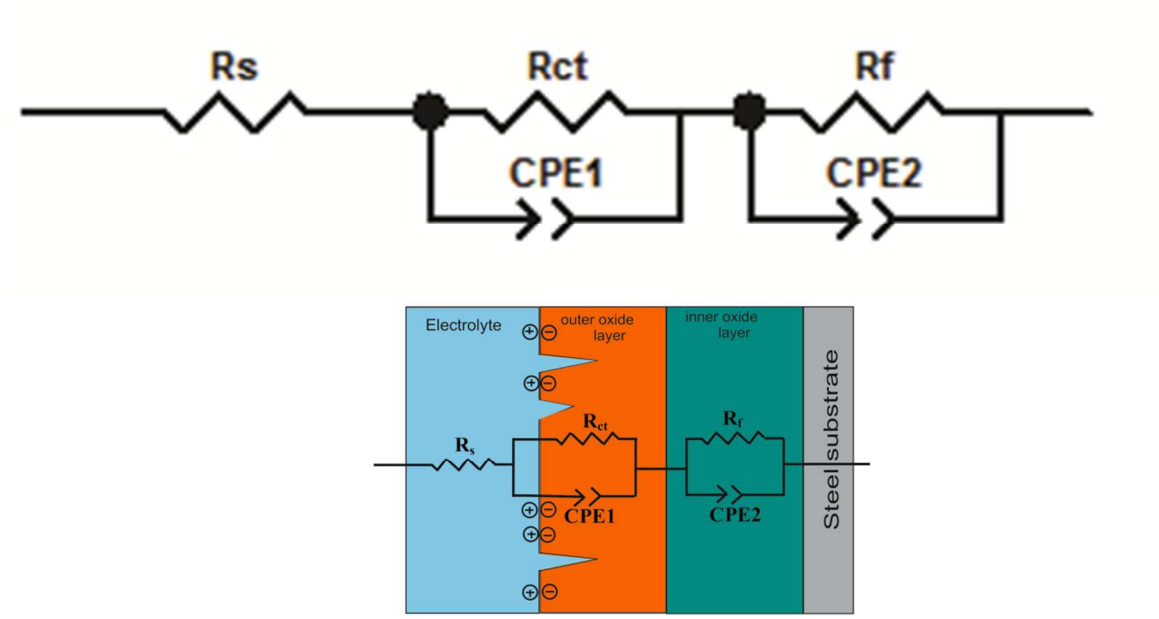

Figure 8a

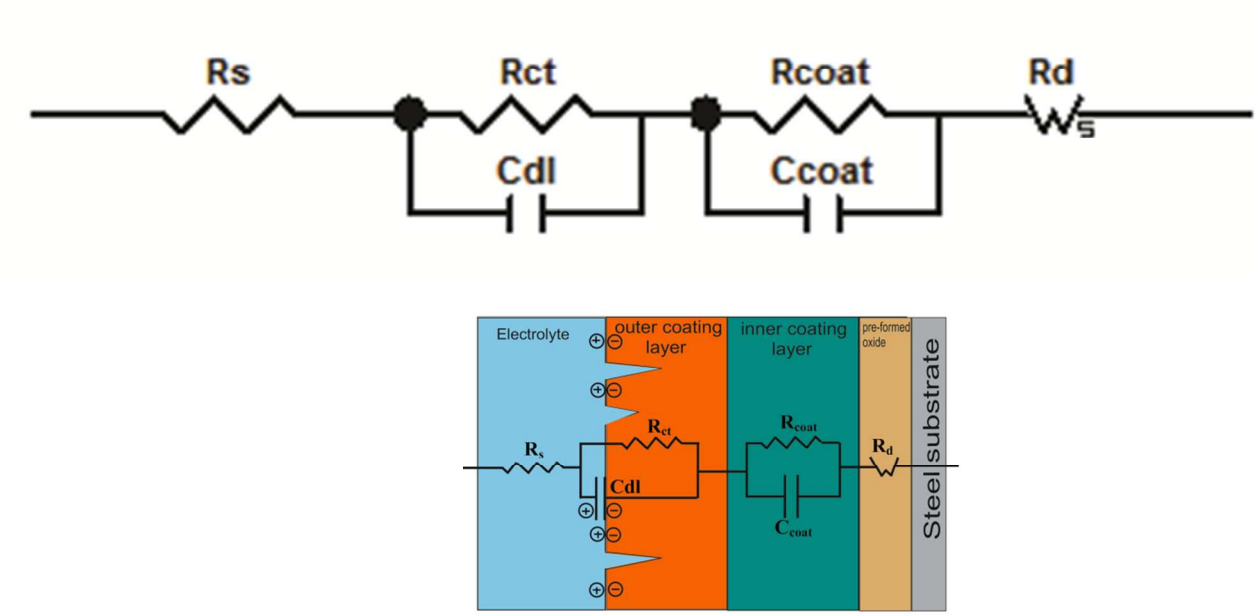

Figure 8b

Table 1. Chemical composition (wt %) of AISI 316.

	C	Cr	Mo	Ni	Mn	Si	P	S	Fe
%	0.080	17.0	2.50	12.0	2.00	1.00	0.045	0.030	Balance

Table 2. Polarization parameters of bare AISI 316, GIG and GIG/CS in 3.5% NaCl at 298 K

	E_{corr} (mV)	i_{corr} ($\mu A\ cm^{-2}\ 10^{-1}$)	β_c (mV/decade)	β_a (mV/decade)	PE (%)
Bare AISI 316	-183.1	4.1	157.3	390.0	0
GIG	-57.1	0.7	110.7	114.5	82.2
GIG/CS	-62.7	0.4	115.2	68.1	89.0

Table 3. Polarization parameters of bare AISI 316, GIG and GIG/CS in 3.5% NaCl at different temperatures

	E_{corr} (mV)	i_{corr} ($\mu A\ cm^{-2}$)	β_c (mV/decade)	β_a (mV/decade)	PE (%)
Bare AISI 316					
298	-183.1	0.4183	157.3	390.0	0
308	-173.0	0.4190	183.3	265.6	0
318	-164.9	0.4479	171.9	188.0	0
328	-182.1	0.5413	266.6	252.7	0
GIG					
298	-57.1	0.0745	110.7	114.5	82.2
308	-40.0	0.0835	117.1	91.5	80.0
318	- 42.1	0.0944	115.8	110.3	78.9
328	-50.4	0.1175	96.7	131.1	78.2
GIG/CS					
298	-62.7	0.0462	115.2	68.1	89.0
308	-65.0	0.0588	86.4	71.8	86.0
318	-74.2	0.0633	113.7	70.5	85.9
328	-78.0	0.0855	118.2	73.1	84.2

Table 4. Impedance parameters of bare AISI 316 after different immersion times in 3.5%NaCl at room temperature.

	$R_s \times 10^1$ (Ω cm^2)	$R_f \times 10^5$ (Ω cm^2)	$R_{ct} \times 10^3$ (Ω cm^2)	CPE1$\times 10^3$ (Ω^{-1} cm^{-2} s^n)	n	CPE2$\times 10^4$ (Ω^{-1} cm^{-2} s^m)	m
After 0 min immersion	4.6	2.9	2.4	2.8	0.9	2.0	0.8
After 10 min immersion	4.3	1.6	0.0017	3.2	0.8	0.25	0.9
After 20 min immersion	1.7	3.1	1.1	3.3	0.8	1.5	0.9
After 30 min immersion	1.2	0.3	0.030	1.2	0.7	0.33	0.8
After 60 min immersion	1.2	8.6	17.9	0.048	0.4	3.6	0.8
After 120 min immersion	3.0	1.6	25.6	1.3	0.7	0.45	0.8

Table 5. Impedance parameters of GIG after different immersion times in 3.5%NaCl at room temperature.

	$R_s \times 10^1$ (Ω cm^2)	$C_{coat} \times 10^{-6}$ (F cm^{-2})	$R_{coat} \times 10^2$ (Ω cm^2)	$C_{dl} \times 10^{-3}$ (F cm^{-2})	$R_{ct} \times 10^4$ (Ω cm^2)	$R_d \times 10^2$ (Ω s$^{-1/2}$)
After 0 min immersion	13.1	6.4	0.62	1.5	3.0	2.1
After 10 min immersion	12.7	7.2	1.03	1.1	3.2	4.3
After 20 min immersion	14.1	9.1	0.82	1.5	7.3	4.9
After 30 min immersion	11.2	7.0	1.32	1.2	1.0	3.4
After 60 min immersion	16.7	7.3	0.64	1.7	4.3	4.1
After 120 min immersion	14.0	5.2	0.49	1.3	3.0	2.5

Table 6. Impedance parameters of GIG/CS after different immersion times in 3.5%NaCl at room temperature.

	$R_s \times 10^1$ (Ω cm^2)	$C_{coat} \times 10^{-6}$ (F cm^{-2})	$R_{coat} \times 10^2$ (Ω cm^2)	$C_{dl} \times 10^{-3}$ (F cm^{-2})	$R_{ct} \times 10^4$ (Ω cm^2)	$R_d \times 10^2$ (Ω s$^{-1/2}$)
After 0 min immersion	1.7	6.7	2.9	1.3	7.4	2.8
After 10 min immersion	2.5	8.2	1.2	1.3	7.2	4.5
After 20 min immersion	1.7	6.8	1.6	1.3	7.7	3.2
After 30 min immersion	2.3	7.5	2.2	1.2	7.3	3.8
After 60 min immersion	2.1	7.6	4.9	1.1	6.7	4.6
After 120 min immersion	1.2	8.7	1.0	1.3	7.5	3.0

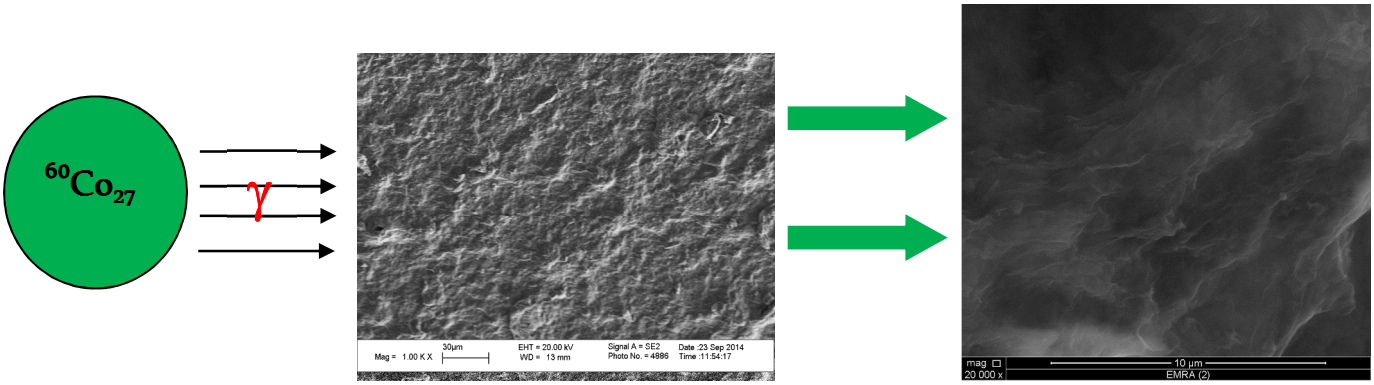

Gamma Source Graphene Oxide Graphene

Graphene prepared by gamma irradiation of GO and used as a coating against pitting corrosion of AISI 316 in NaCl